Expression of Amyloidogenic Transthyretin Drives Hepatic Proteostasis Remodeling in an Induced Pluripotent Stem Cell Model of Systemic Amyloid Disease

Richard M. Giadone,[1,6] Derek C. Liberti,[1,6] Taylor M. Matte,[1] Jessica D. Rosarda,[3] Celia Torres-Arancivia,[2] Sabrina Ghosh,[1] Jolene K. Diedrich,[3] Sandra Pankow,[3] Nicholas Skvir,[1] J.C. Jean,[1,4] John R. Yates III,[3] Andrew A. Wilson,[1,4] Lawreen H. Connors,[2] Darrell N. Kotton,[1,4] R. Luke Wiseman,[3] and George J. Murphy[1,5,*]

[1]Center for Regenerative Medicine of Boston University and Boston Medical Center, 670 Albany Street, 2nd Floor, Boston, MA 02118, USA
[2]Alan and Sandra Gerry Amyloid Research Laboratory, Amyloidosis Center, Boston University School of Medicine, Boston, MA, USA
[3]Department of Molecular Medicine, The Scripps Research Institute, La Jolla, CA, USA
[4]The Pulmonary Center and Department of Medicine, Boston University School of Medicine, Boston, MA, USA
[5]Section of Hematology and Oncology, Department of Medicine, Boston University School of Medicine, Boston, MA, USA
[6]Co-first author
*Correspondence: gjmurphy@bu.edu
https://doi.org/10.1016/j.stemcr.2020.07.003

SUMMARY

The systemic amyloidoses are diverse disorders in which misfolded proteins are secreted by effector organs and deposited as proteotoxic aggregates at downstream tissues. Although well described clinically, the contribution of synthesizing organs to amyloid disease pathogenesis is unknown. Here, we utilize hereditary transthyretin amyloidosis (ATTR amyloidosis) induced pluripotent stem cells (iPSCs) to define the contribution of hepatocyte-like cells (HLCs) to the proteotoxicity of secreted transthyretin (TTR). To this end, we generated isogenic, patient-specific iPSCs expressing either amyloidogenic or wild-type TTR. We combined this tool with single-cell RNA sequencing to identify hepatic proteostasis factors correlating with destabilized TTR production in iPSC-derived HLCs. By generating an ATF6 inducible patient-specific iPSC line, we demonstrated that enhancing hepatic ER proteostasis preferentially reduces the secretion of amyloidogenic TTR. These data highlight the liver's capacity to chaperone misfolded TTR prior to deposition, and moreover suggest the potential for unfolded protein response modulating therapeutics in the treatment of diverse systemic amyloidoses.

INTRODUCTION

The systemic amyloid diseases represent a class of devastating protein-folding disorders affecting more than 1 million individuals worldwide (Blancas-Mejia and Ramirez-Alvarado, 2013, Buxbaum, 2004; Falk et al., 1997; Merlini and Westermark, 2004; Wechalekar et al., 2016). In these diseases, proteins containing destabilizing mutations are produced and secreted from an effector organ into circulation. In the blood, these proteins undergo misfolding and subsequent aggregation into toxic oligomers, depositing at distal tissues, and resulting in organ dysfunction. Systemic amyloid diseases result from the misfolding of over 15 structurally distinct proteins, a majority of which are synthesized by the liver. A prominent example of this family of diseases is hereditary transthyretin amyloidosis (ATTR amyloidosis).

Hereditary ATTR amyloidosis is an autosomal dominant disorder that can result from over 100 described mutations in the transthyretin (*TTR*) gene (Ando et al., 2005; Benson, 2012; Gertz et al., 2015; Reixach et al., 2004; Ruberg and Berk, 2012). Normally, TTR is produced in the liver, with minimal local synthesis by retinal pigment epithelial cells of the eye and choroid plexus of the brain (Ando et al., 2005; Benson, 2012; Reixach et al., 2004; Ruberg and

Berk, 2012). Normally, TTR produced by the liver forms a tetramer and is secreted, serving as the major serum transporter of retinol binding protein charged with retinol (Ando et al., 2005; Benson, 2012; Gertz et al., 2015; Reixach et al., 2004; Ruberg and Berk, 2012). In ATTR amyloidosis, TTR mutations decrease the stability of the tetramer, leading to monomerization and misfolding of TTR subunits. Misfolded monomers then aggregate to form proteotoxic oligomers and amyloid fibrils at target tissues including the heart and peripheral nerves (Ando et al., 2005; Benson, 2012; Gertz et al., 2015; Reixach et al., 2004; Ruberg and Berk, 2012). Standards of care for ATTR amyloidosis patients include kinetic stabilizers that bind the tetrameric protein, limiting monomerization, and downstream aggregation as well as recently developed RNA interference (RNAi)-based therapeutics that inhibit translation of TTR transcripts (Adams et al., 2018; Ando et al., 2016; Benson et al., 2018; Berk et al., 2013; Butler et al., 2016; Buxbaum, 2019; Gertz et al., 2015; Maurer et al., 2017, 2018). Despite success in clinical trials for such drugs, not all patients respond equally and effectively, likely attributed to the inherited *TTR* mutation and the underlying genetic background of the individual (Ando et al., 2016; Berk et al., 2013; Buxbaum, 2019; Gertz et al., 2015; Maurer et al., 2017, 2018). Due to their multi-tissue etiologies, systemic

amyloid diseases such as ATTR amyloidosis prove difficult to study, while until only recently, mouse models have failed to recapitulate key aspects of human TTR amyloid pathology (Buxbaum, 2009; Giadone et al., 2018; Kan et al., 2018; Leung et al., 2013; Leung and Murphy, 2016; Li et al., 2018; Sousa et al., 2002). To study disease pathogenesis in the genetic context of the patient, we differentiated patient-specific ATTR amyloidosis induced pluripotent stem cells (iPSCs) into effector hepatocyte-like cells (HLCs) that produce and secrete destabilized TTR (Giadone et al., 2018; Leung et al., 2013; Leung and Murphy, 2016).

Traditionally, ATTR amyloidosis livers have been thought to be normal, as toxicity occurs at downstream target organs (Ando et al., 2005; Benson, 2012; Blancas-Mejia and Ramirez-Alvarado, 2013; Buxbaum, 2004; Falk et al., 1997; Gertz et al., 2015; Merlini and Westermark, 2004; Reixach et al., 2004; Ruberg and Berk, 2012; Wechalekar et al., 2016). Despite this, however, many studies suggest the capacity for the liver to contribute to the deposition of amyloidogenic proteins at distal target tissues. Recipients of domino liver transplantations (DLTs), for instance, receive a liver from an ATTR amyloidosis donor and in turn show accelerated TTR fibril accumulation on target organs (<10 years post transplant) (Ericzon, 2007; Llado et al., 2010; Misumi et al., 2016; Muchtar et al., 2017; Stangou et al., 2005; Yamamoto et al., 2007). Furthermore, *in vivo* mouse experiments demonstrate that the deposition of TTR in the hearts of old mice correlates with altered expression of numerous hepatic proteostasis genes (Buxbaum et al., 2012). Together, these results implicate the liver in the pathogenesis of systemic amyloid diseases such as ATTR amyloidosis.

Here, we utilize a patient-specific iPSC-based model of ATTR amyloidosis to investigate the contribution of hepatic proteostasis and disease-modifying factors to the distal toxicity observed in patients. Recent attempts have been made to identify transcriptional differences between ATTR amyloidosis and wild-type iPSC-derived HLCs via qRT-PCR (Niemietz et al., 2018). Problematically, the maturational status of examined cells in these studies was not taken into account, and reported results likely reflect distinct differentiation efficiencies between lines. In turn, differences in human ATTR amyloidosis HLCs resulting solely from mutant TTR expression remain elusive. Utilizing gene editing in combination with single-cell RNA sequencing (scRNA-seq), we define distinct transcriptional profiles in syngeneic corrected and uncorrected ATTR amyloidosis iPSC-derived HLCs. In turn, we show that expression of the most proteotoxic TTR variant in HLCs correlates with expression of genes inversely implicated in the toxic aggregation of TTR, including transferrin (*TF*) and target genes of the unfolded protein response (UPR). To assess the consequence of functional activation of the adaptive UPR within HLCs expressing mutant TTR, we generated an ATF6-inducible patient-specific iPSC line. We further utilize this tool to demonstrate that exogenous ATF6 activation preferentially reduces HLC secretion of mutant, amyloidogenic TTR.

RESULTS

TTR Is a Major Differentially Expressed Gene throughout Human Hepatic Specification

Recent work from our group demonstrated the emergence of a stage-dependent disease signature of hepatic-specified pluripotent stem cells (PSCs) (Wilson et al., 2015). In these experiments, microarray analyses were performed on cells isolated at days 0, 5, and 24 of hepatic differentiation. Post hoc analysis of these data revealed *TTR* to be the second most differentially expressed gene comparing differentiated HLCs with PSCs (Figure 1A). To confirm this, we performed qRT-PCR on RNA isolated from day-24 HLCs, demonstrating significant upregulation of *TTR* compared with iPSCs (Figure 1B). These data demonstrate that TTR is a robust marker of hepatic specification and can be used to normalize PSC-derived hepatic differentiations.

Gene Editing of ATTR Amyloidosis iPSCs Eliminates Secretion of Mutant TTR[L55P] and Decreases Target Cell Toxicity

As noted above, *TTR* is one of the most differentially expressed genes in HLC differentiation, suggesting it might serve as an excellent candidate locus to target and generate a hepatic specification reporter iPSC line. To this end, we employed TALEN-mediated gene editing to manipulate an iPSC line derived from a patient with the Leu55→Pro (TTR[L55P]) mutation, one of the most proteotoxic disease-causing variants (Jacobson et al., 1992; Lashuel et al., 1999; McCutchen et al., 1993). To implement a broadly applicable gene-correction strategy, we targeted the ATG start site of the endogenous, mutant *TTR* allele, introducing a wild-type TTR coding sequence, followed by a 2A self-cleaving peptide and *eGFP* coding sequence (Figure 1C). Inclusion of a 2A peptide allows for transcription of a single mRNA that ultimately results in two independent TTR and GFP proteins via a post-translational cleavage event. As a result of this targeting methodology, transcription and translation of mutant *TTR* is abrogated via introduction of an artificial STOP codon and poly(A) sequence, and replacement with a wild-type *TTR* coding sequence (Figure 1C). Importantly, this universal gene-correction strategy provides a singular technique for correcting all known *TTR* genetic lesions while simultaneously obviating concerns regarding haploinsufficiency via replacement of the endogenous mutant *TTR* allele with a wild-type copy.
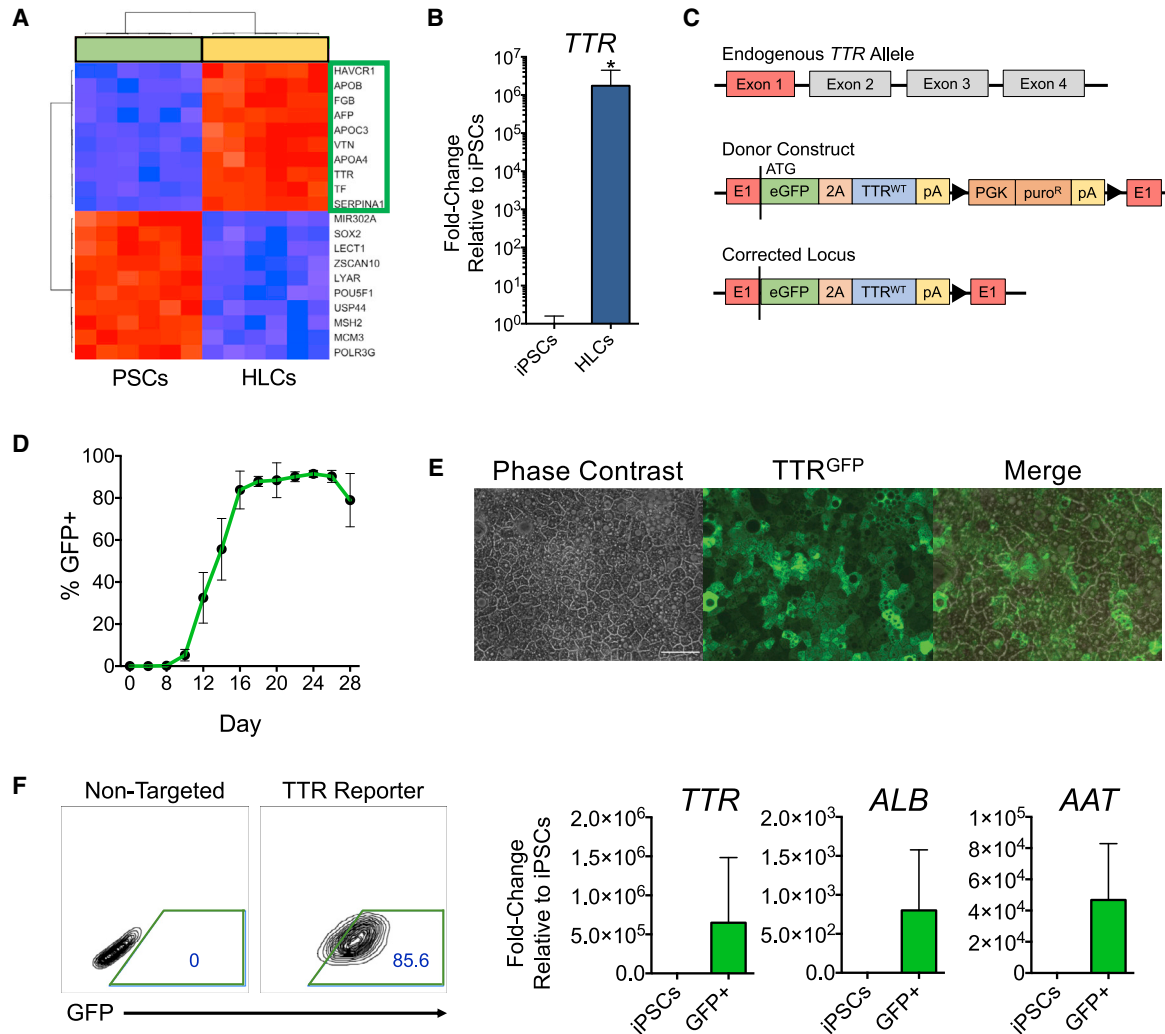
Figure 1. Creation of a TTR Promoter-Driven Hepatic Specification Reporter iPSC Line and Universal Gene-Editing Strategy for Hereditary ATTR Amyloidosis

(A) Undifferentiated PSCs and day-24 HLCs (green and yellow columns, respectively) form distinct, independent clusters by microarray analysis. Top 10 transcripts upregulated in HLCs are labeled on the y axis, highlighted by green box. Top 10 transcripts downregulated in HLCs are labeled on the y axis (below). Top differentially expressed genes were determined by one-way ANOVA.

(B) qRT-PCR validating microarray finding that expression of *TTR* mRNA is significantly upregulated in day-24 HLCs compared with un-differentiated iPSCs; fold change calculated over undifferentiated iPSCs (n = 3 independent differentiations, *p < 0.05, unpaired t test for significance, error bars denote standard deviation).

(C) Schematic representation of the gene targeting strategy. Black triangles flank Cre-excisable *LoxP* sites.

(D) Flow-cytometry-based time course of GFP⁺ cells that appear throughout hepatic specification of targeted iPSCs (n = 3 independent differentiations, error bars denote standard deviation).

(E) Phase (left) and fluorescence (middle, right) microscopy images of day-26 reporter iPSC-derived HLCs. Images taken at 20× magnification. Scale bar, 100 μm.

(F) Expression of hepatic markers in sorted day-16 GFP⁺ HLCs; fold change calculated over undifferentiated iPSCs (n = 5 independent differentiations, error bars denote standard deviation).

Additional information regarding generation and characterization of corrected iPSCs can be found in Figure S1.

Using this TTR reporter line, we then measured the kinetics of GFP expression throughout HLC differentiation by flow cytometry. In doing so, we found that expression of GFP peaked at approximately day 16 of a 24-day specification protocol (Figure 1D). By day 24, HLCs exhibited cobblestone-like morphology, and the majority of cells
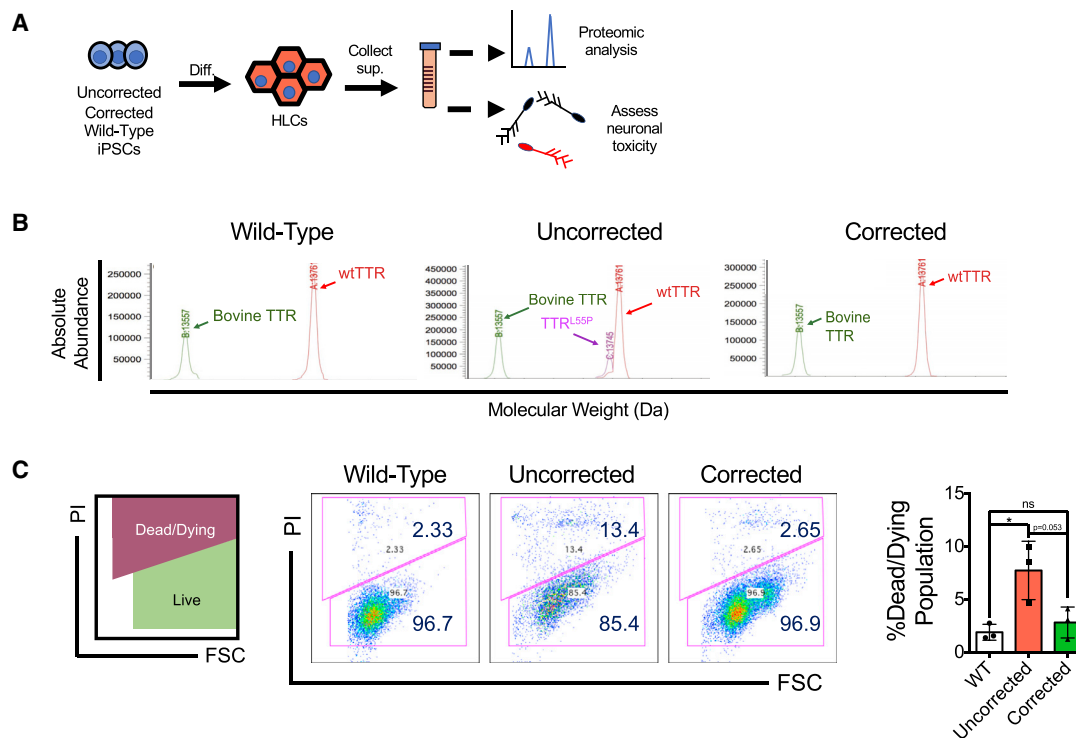
Figure 2. Gene-Edited iPSC-Derived HLCs No Longer Produce Neurotoxic, Destabilized TTR Variants

(A) Experimental overview depicting interrogation of wild-type, TTR^{L55P}, and corrected iPSC-derived HLC supernatants and determination of their requisite downstream effects on neuronal target cells.

(B) LC-MS analyses of supernatant from wild-type, TTR^{L55P}, and corrected iPSC-derived HLCs. Red trace, TTR^{WT}; pink trace, destabilized TTR^{L55P} variant. Bovine TTR (green) is present in media supplements. The molecular weight of each species is denoted in daltons.

(C) SH-SY5Y cells were dosed for 7 days with conditioned iPSC HLC-derived supernatant from wild-type, TTR^{L55P}, or corrected conditions. Cell viability was determined via PI staining (n = 3 independent dosing trials of SH-SY5Y cells using conditioned supernatant from independent hepatic differentiations, unpaired t test for significance comparing uncorrected and corrected conditions, error bars denote standard deviation).

expressed GFP (Figure 1E). To further validate this reporter line and ensure that GFP expression correlated with the expression of TTR as well as other hepatic specification markers, we sorted day-16 GFP$^+$ HLCs and assayed them via qRT-PCR. GFP$^+$ cells expressed high levels of *TTR* as well as other hepatic specification markers such as *AAT* and *ALB* (Figure 1F), suggesting that our corrected reporter cell line labels maturing hepatic lineage cells during specification.

We further examined the ability of this strategy to eliminate the production of destabilized, disease-causing TTR, as well as alleviate downstream toxicity (outlined in Figure 2A). To this end, we differentiated wild-type, corrected, and non-targeted, heterozygous TTR^{L55P} iPSCs into HLCs. Conditioned supernatant from each line was harvested after culturing cells for 72 h in hepatic specification medium beginning on day 16 of the differentiation. We used liquid chromatography combined with mass spectrometry

(LC-MS) to show that TTR immunopurified from wild-type iPSC-derived hepatic supernatants contained TTR^{WT}, but not TTR^{L55P}, while supernatants collected from patient iPSC-derived HLCs contained both TTR^{WT} and TTR^{L55P} (Figure 2B). Supernatant from corrected iPSC-derived HLCs revealed complete elimination of TTR^{L55P} while levels of TTR^{WT} remained unperturbed (Figure 2B). Importantly, the two-amino-acid overhang on the N-terminal portion of TTR, resulting from the post-translational cleavage of the 2A peptide, was removed with the TTR signal peptide through normal protein processing in the ER (made evident by the identical molecular weights observed for endogenous and exogenous TTR^{WT}), showing that TTR^{WT} from our donor construct is indistinguishable from the endogenous protein.

As decreasing circulating levels of destabilized TTR results in decreased peripheral organ dysfunction (Ericzon et al., 2000; Hemming et al., 1998; Herlenius et al., 2004), we

sought to determine the efficacy of our iPSC-based gene correction in decreasing toxicity in a cell-based model. To accomplish this, we dosed a neuroblastoma cell line (SH-SY5Y) with conditioned supernatant generated from mutant TTR^{L55P}, corrected, or wild-type HLCs, and surveyed them for toxicity. In these assays, SH-SY5Y cells dosed with mutant hepatic supernatant displayed an increase in propidium iodide-positive (PI$^+$) cells compared with those dosed with wild-type supernatant (Figure 2C). Cells dosed with corrected supernatant, however, exhibited a modest, though not statistically significant (p = 0.0525), decrease in toxicity comparable with levels observed in the wild-type control dosing sample (Figure 2C). These results suggest that the proposed gene-correction strategy ameliorates TTR-mediated toxicity via reductions in the hepatic secretion of destabilized TTR.

Single-Cell RNA Sequencing Reveals a Hepatic Gene Signature Associated with the Production of Destabilized TTR^{L55P}

Historically, it has been thought that the livers of patients with ATTR amyloidosis are unaffected during disease pathogenesis (Ando et al., 2005; Benson, 2012; Blancas-Mejia and Ramirez-Alvarado, 2013; Buxbaum, 2004; Falk et al., 1997; Gertz et al., 2015; Merlini and Westermark, 2004; Reixach et al., 2004; Ruberg and Berk, 2012; Wechalekar et al., 2016). Recent work, however, calling into question the use of donor organs from ATTR amyloidosis patients for DLT procedures challenges this notion, indicating that genetic or aging-related perturbations to the liver could influence the toxic extracellular aggregation and deposition of TTR on peripheral target tissues (Chen et al., 2014, 2016; Genereux et al., 2015; Plate et al., 2016; Shoulders et al., 2013). To define specific hepatic proteins and pathways associated with the production of destabilized amyloidogenic TTR variants, we coupled our TTR reporter system with single-cell RNA sequencing (scRNA-seq) to compare mRNA expression profiles in syngeneic iPSC-derived HLCs with or without the TTR^{L55P} mutation. In addition to our corrected TTR reporter iPSC line, we also constructed a reporter cell line where our TTR-GFP donor construct was targeted to the wild-type TTR allele in the same TTR^{L55P} parental iPSC line. As a result, we created two syngeneic, TTR-promoter-driven hepatic specification reporter iPSC lines, where the only difference is the presence or absence of the disease-causing TTR^{L55P} mutation (henceforth referred to as uncorrected and corrected cells, respectively). To compare HLCs ± TTR^{L55P}, we subjected uncorrected and corrected reporter iPSCs to our hepatic specification protocol until TTR expression had plateaued (at day 16 of the differentiation) (Figure 1D). To control for the inherent heterogeneity of iPSC differentiations, we purified GFP$^+$ cells by fluorescence-activated cell sorting (FACS) to select for cells undergoing hepatic specifi-

cation (i.e., at similar stages in their developmental trajectories). Employing scRNA-seq in combination with our FACS-based purification strategy, we significantly reduced the potential for differences in corrected and uncorrected cells resulting from maturational status. Transcriptomic profiling was subsequently performed at single-cell resolution via the Fluidigm C1 platform (outlined in Figure 3A).

Day-16 uncorrected and corrected HLCs formed clear and distinct groups by supervised principal component analysis (PCA), with 92 genes differentially expressed between the two groups (Figures 3B–3D and Data S1) (significance determined via one-way ANOVA, false discovery rate [FDR] cutoff <0.05). These analyses identified increased expression of distinct genes and pathways previously shown to influence extracellular aggregation of destabilized TTRs in uncorrected but not corrected HLCs (vide infra) (Chen et al., 2014, 2016; Genereux et al., 2015; Plate et al., 2016; Shoulders et al., 2013).

Transferrin Expression Is Significantly Increased in Uncorrected HLCs and May Represent a Chaperone for Destabilized TTR

The top differentially expressed gene in uncorrected HLCs is the iron transporter, *TF* (Figures 3C and 3D). Although *TF* is a known hepatic lineage marker, no other hepatic markers (including *TTR*, *ALB*, *AFP*, *HNF4A*, *FOXA1*, *GATA4*, *SERPINA1*, *FGB*, *DUOX2*, *A2M*, *TGM2*, *HAVCR1*, and *GATA6*) are differentially expressed between corrected and uncorrected HLCs, suggesting that the differential expression of *TF* is not simply due to the differentiation status of individual lines (Figures 3D and S2).

Interestingly, previous studies have demonstrated the ability of TF to act as a chaperone in the context of other amyloid disorders such as Alzheimer's disease (AD) as well as to physically interact with TTR fibrils *in vivo* (Loeffler et al., 1995). As a result, we sought to assess the capacity for TF to act as a chaperone for misfolding TTR and in turn prevent TTR fibril formation. To this end, we performed an *in vitro* fibril formation assay whereby the formation of congophilic fibrils from recombinant human TTR^{L55P} was assessed with or without the addition of TF (Figure 4A). In doing so, iron-free (apo-) TF at physiologically relevant concentrations reduced the amount of congophilic species formed by approximately 60% (Figure 4B). Notably, iron-bound transferrin, at similar concentrations, was found to have no effect on fibril formation (data not shown), perhaps owing to well-documented iron binding-induced conformational changes (Yang et al., 2012).

Uncorrected HLCs Show Increased Activation of Protective UPR-Associated Signaling Pathways

Analysis of our scRNA-seq data also identified increased expression of multiple UPR-regulated ER proteostasis
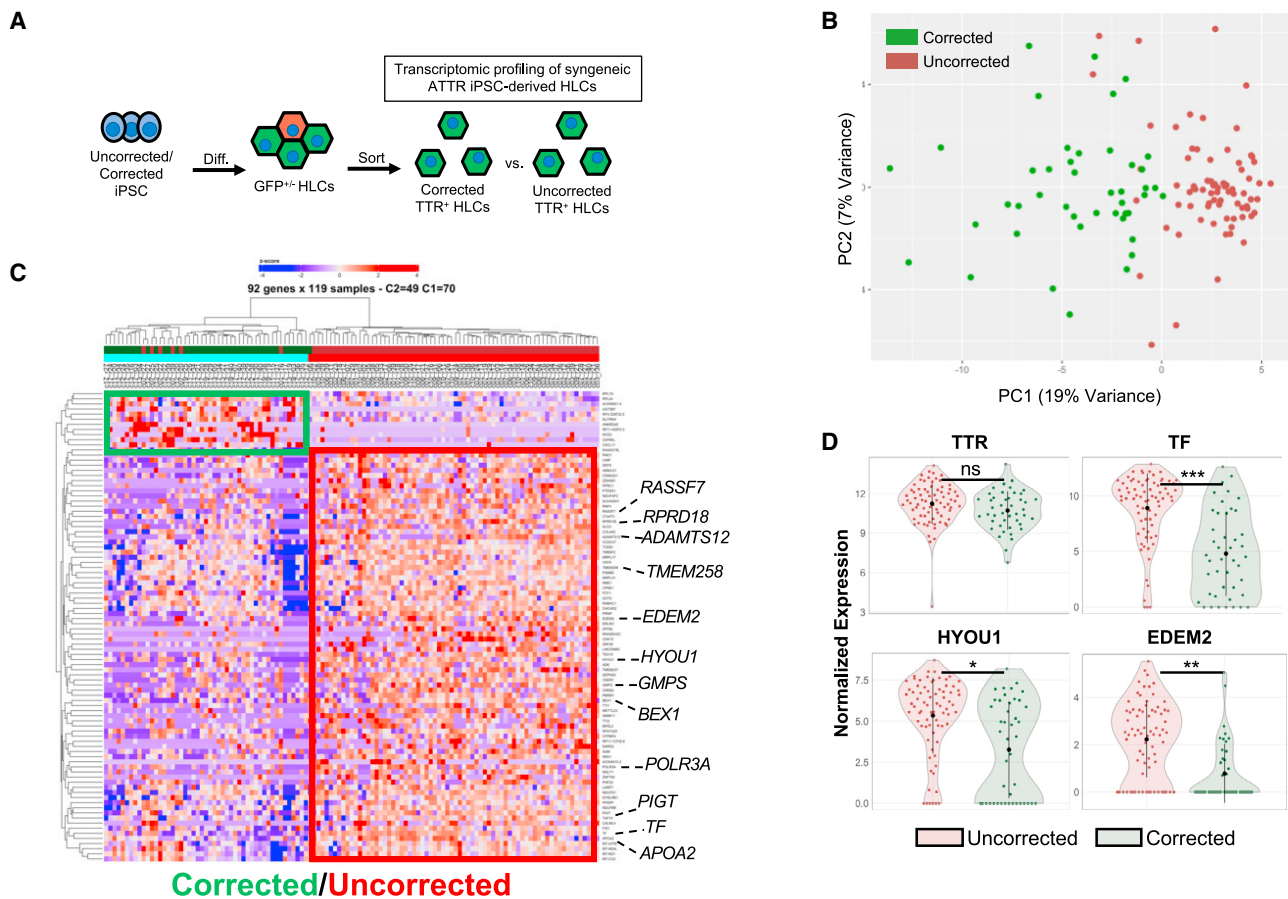
Figure 3. Single-Cell RNA Sequencing of Corrected versus Uncorrected Syngeneic iPSC-Derived HLCs Reveals a Hepatic Gene Signature

(A) Experimental schematic for the transcriptomic comparison of uncorrected (TTR^{L55P}-expressing) and corrected syngeneic iPSC-derived HLCs at day 16 of the hepatic specification protocol.

(B) Uncorrected (red) and corrected (green) populations form distinct groups by supervised principal component analysis (PCA). Supervised PCA was constructed using the top 500 differentially expressed genes by FDR.

(C) Heatmap depicting the 92 genes differentially expressed between uncorrected and corrected populations (one-way ANOVA, FDR cutoff <0.05). Columns represent individual cells, green bar denotes corrected cells, red bar denotes uncorrected cells. Rows represent differentially expressed genes. The top 10 genes by fold change (uncorrected over corrected) as well as proteostasis factor *EDEM2* are highlighted on the y axis.

(D) Violin plots representing relative expression levels of *TTR*, potential mediators of TTR fibrillogenesis (*TF*) and UPR target genes (*HYOU1*, *EDEM2*). (FDR determined via one-way ANOVA; *FDR < 0.05, **FDR < 0.005, ***FDR < 0.0005.)

factors (e.g., *HYOU1* and *EDEM2*; Figures 3C and 3D) in HLCs expressing TTR^{L55P}. Increases in expression of said factors suggest that the presence of the destabilized TTR^{L55P} protein challenges the proteostasis environment and in turn activates the UPR.

To better define the impact of TTR^{L55P} expression on ER stress and UPR activation, we used gene set enrichment analysis (GSEA) to define the extent of UPR activation in our uncorrected iPSC-derived HLCs. This analysis revealed modest activation of the adaptive IRE1/XBP1s and

ATF6 UPR transcriptional signaling pathways, with no significant activation of the pro-apoptotic PERK UPR pathway (Figure 4C). We further confirmed IRE1/XBP1s activation in two independent patient-specific iPSC-derived HLCs by monitoring IRE1-dependent *XBP1* splicing (Figures 4D–4F). As a positive control, cells were dosed with the global UPR activator thapsigargin (Tg). These results demonstrate that expression of amyloidogenic TTR^{L55P} promotes adaptive remodeling of ER proteostasis through the IRE1/XBP1s and ATF6 UPR signaling pathways.
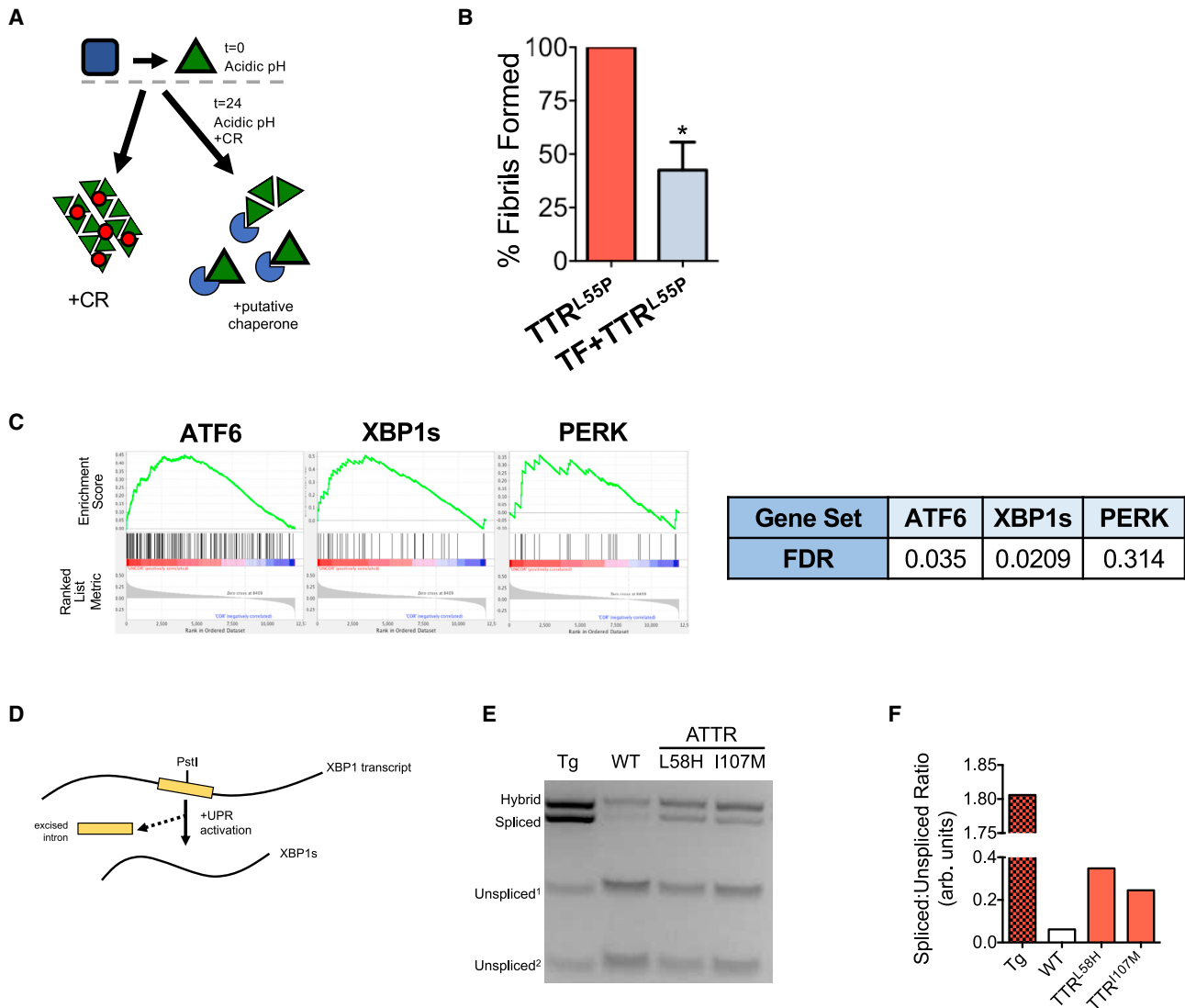
Figure 4. Assessment of TF Chaperone Capacity and Functional Validation of XBP1 Activation in ATTR Amyloidosis HLCs

(A) Experimental outline for assessing TF's *in vitro* ability to prevent the formation of congophilic species from recombinant TTR[L55P].

(B) Percentage of TTR[L55P] fibrils formed as determined by amount of Congo red bound after 24-h incubation of recombinant protein under fibril forming conditions (n = 5 independent *in vitro* formation of fibrils, **p < 0.005, unpaired t test for significance comparing apo-TF condition with TTR[L55P] alone, error bars denote standard deviation).

(C) GSEA depicting significant enrichment of adaptive UPR machinery (ATF6, XBP1s) but not PERK target genes in uncorrected HLCs. In these analyses, 100 uncorrected and 60 corrected cells were studied.

(D) Depiction of XBP1 splicing in the presence of ER stress and UPR activation.

(E) PstI analytical digest of amplified XBP1 transcripts from iPSCs treated with Tg, wild-type iPSC-derived HLCs (WT), and ATTR HLCs differentiated from two patient-specific iPSC lines (L58H and I107M). Hybrid band represents a PstI-resistant spliced-unspliced XBP1 product generated via PCR protocol.

(F) Densitometric quantitation of PstI-digested XBP1 transcripts. Ratio determined by $\dfrac{XBP1_{spliced}}{XBP1_{unspliced1} + XBP1_{unspliced2}}$.

Hepatic Activation of ATF6 Signaling Selectively Reduces Secretion of Destabilized TTR[L55P]

We next determined the consequence of functional activation of adaptive UPR-associated signaling pathways in ATTR amyloidosis patient-specific HLCs expressing mutant, destabilized TTR. To accomplish this, we introduced an ATF6-inducible donor construct into our previously described heterozygous TTR[L55P] patient-specific iPSC line.
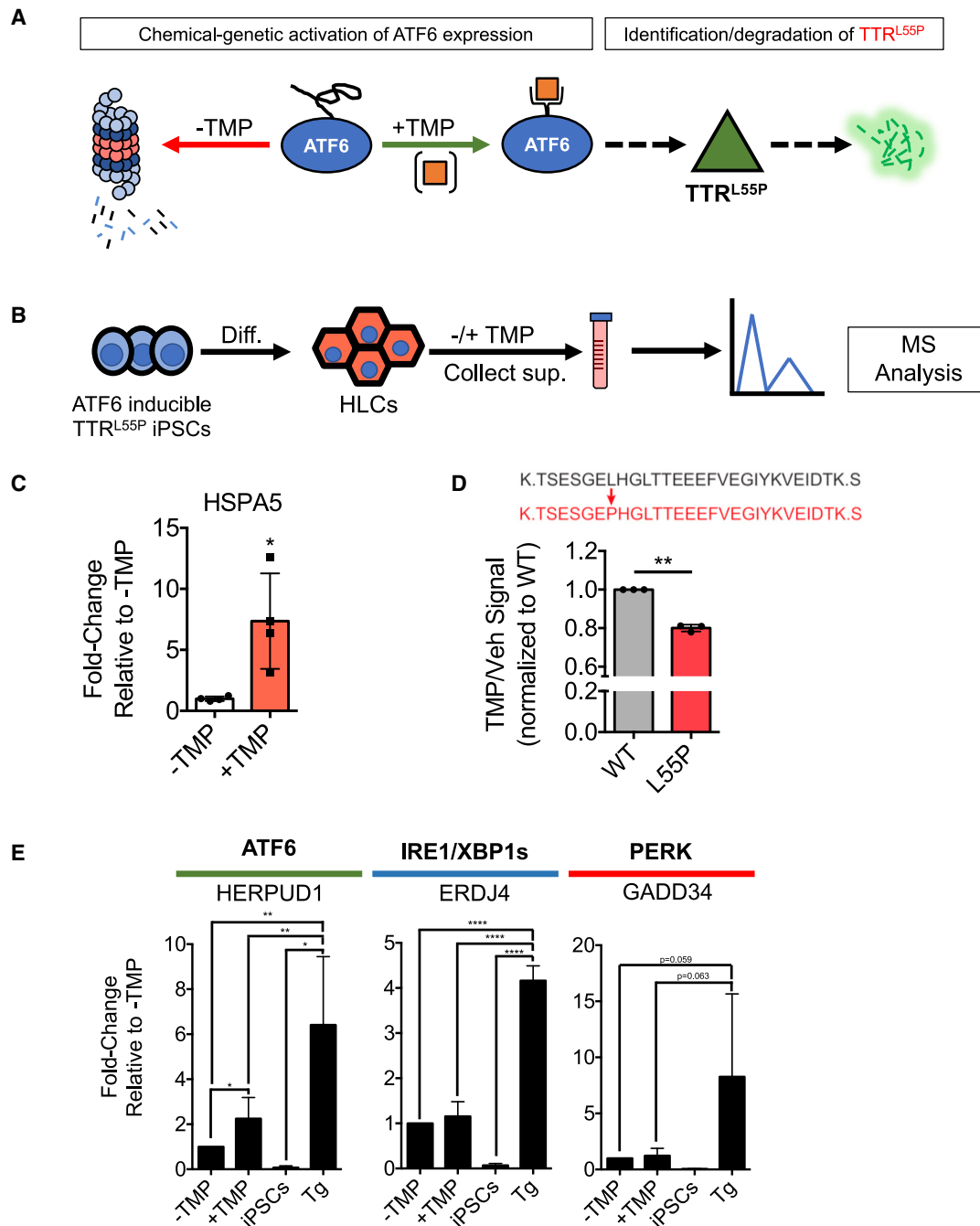
Figure 5. Hepatic Stress-Independent, Branch-Specific Activation of Adaptive UPR-Associated ATF6 Signaling Results in the Targeting and Selective Reduction in the Secretion of Destabilized TTR[L55P]

(A) A chemical inducible system for activating ATF6 signaling in TTR[L55P] iPSC-derived cell types. In the absence of chemical chaperone TMP, DHFR.ATF6 is degraded. Upon addition of TMP, DHFR.ATF6 is stabilized and targets and attenuates the secretion of misfolded TTRs.

(B) ATF6-inducible iPSCs were differentiated into HLCs. TMP was added, and conditioned supernatant was collected and interrogated for the presence and relative abundance of different TTR species via LC-MS/MS.

(C) ATF6 target gene *HSPA5* was found to be significantly upregulated upon addition of TMP by qRT-PCR (n = 4 independent differentiations, *p < 0.05, unpaired t test for significance comparing −TMP to +TMP conditions, error bars denote standard deviation).

(D) LC-MS/MS was used to directly detect the presence of TTR[WT] (upper peptide sequence, black) and TTR[L55P] (lower peptide sequence, orange) peptides in conditioned supernatant in the presence and absence of TMP. Abundance of TTR[L55P] was found to significantly

In these cells, the coding sequence for the active N-terminal bZIP transcription factor domain of ATF6 is fused to a destabilized dihydrofolate reductase (DHFR) tag as previously described (Shoulders et al., 2013). In the absence of the chemical chaperone trimethoprim (TMP), the DHFR.ATF6 protein product is targeted for degradation via the ubiquitin proteasome system (Figure 5A). Upon administration of TMP, the DHFR domain is stabilized, allowing dosable, stress-independent activation of ATF6 transcriptional activity (Figure 5A). ATF6-inducible iPSCs were differentiated into HLCs and subsequently dosed with TMP, beginning on day 15 of hepatic specification (outlined in Figure 5B). Administration of TMP induced selective expression of the ATF6 target genes $HSPA5$ and $HERPUD1$, but not IRE1/XBP1s or PERK target genes (e.g., $ERDJ4$ and $GADD34$, respectively) (Figures 5C and 5E), confirming selective TMP-dependent ATF6 activation in these HLCs. We then collected conditioned media incubated on patient iPSC-derived HLCs dosed with or without TMP for 72 h and monitored the relative populations of TTR^{WT} and TTR^{L55P} by MS. We initially showed that the relative recovery of TTR^{L55P} from immunoprecipitations of media prepared on HLCs treated with TMP was reduced relative to TTR^{WT}, suggesting reduced secretion of this destabilized TTR variant induced by stress-independent ATF6 activation (Figures S3A and S3B). To ensure that the observed decreases in hepatic secretion of TTR^{L55P} were not due to differences in our ability to pull down different TTR species (e.g., wild-type versus mutant as well as various conformational states), we employed an unbiased MS approach not relying on immunoprecipitation. In line with this, we performed tandem mass tag (TMT)/LC-MS/MS quantitative proteomics to directly monitor the relative amount of peptides derived from TTR^{WT} or TTR^{L55P} in these conditioned media (Figure 5D). Using this quantitative approach, we showed that TMP-dependent ATF6 activation preferentially reduces levels of destabilized TTR^{L55P} by 25% relative to TTR^{WT} in HLC conditioned media. This demonstrates that stress-independent ATF6 activation selectively reduces secretion of destabilized, amyloidogenic TTR^{L55P} in patient iPSC-derived HLCs. To assess the ability of ATF6 activation to limit toxicity resulting from prolonged ER stress, we exposed cells to Tg for 5 days. At the same time, we also activated ATF6 signaling (via addition of TMP) or inhibited ATF6 signaling (via addition of the small molecule ceapin-A7 [CP7]) (Gallagher et al., 2016; Gallagher and Walter, 2016; Torres et al., 2019). In doing so, we demonstrated that branch-specific activation of ATF6 signaling protects iPSC-derived HLCs from morphological defects resulting from prolonged exposure to severe ER stress via addition of Tg (Figures S4A and S4B).

DISCUSSION

Through the use of gene editing and scRNA-seq, we defined distinct transcriptional profiles for HLCs expressing destabilized TTR^{L55P}. We hypothesized that hepatic production of destabilized TTRs results in the upregulation of stress-responsive proteostasis factors that regulate the secretion and subsequent aggregation of destabilized TTR variants such as TTR^{L55P}. Our scRNA-seq experiment revealed that uncorrected HLCs exhibited differential expression of 92 genes compared with syngeneic HLCs, where the only difference is the absence of expression of the mutant TTR. In line with our rationale, we identified many instances in which mutant HLCs upregulated expression of well-documented ER stress-associated proteostasis factors involved in regulating protein secretion (e.g., $HYOU1$ and $EDEM2$).

Interestingly, TF was found to be the most upregulated gene in uncorrected, TTR^{L55P}-expressing HLCs. Despite limited prior evidence for TF as a chaperone for misfolded TTRs, recent work implicates its chaperone capacity in other amyloid disorders such as AD, noting increased protein-level expression in the prefrontal cortices of AD patients compared with elderly, non-diseased individuals (Raditsis et al., 2013). Moreover, recent work demonstrated the ability of TF to physically interact with and prevent the self-assembly and toxicity of β-amyloid peptide oligomers, the amyloidogenic protein species in AD (Giunta et al., 2004; Raditsis et al., 2013). At the same time, recent $in\ vivo$ data have demonstrated physical interactions between TF and TTR amyloid fibrils (Ohta et al., 2018). Through the use of congophilic fibril formation assays, we demonstrated that iron-free TF at physiologically relevant levels decreased $in\ vitro$ TTR^{L55P} fibril formation by approximately 60%, implicating TF as a chaperone for hepatic TTRs. These observations, together with our scRNA-seq and biochemical data, suggest the possibility that TF plays a similar protective role in ATTR amyloidosis. In this model, HLCs producing mutant TTR may express higher levels of TF to prevent toxicity and/or fibril formation.

decrease upon activation of ATF6 signaling by ∼25% relative to TTR^{WT}. Quantities of each peptide were normalized to TTR^{WT} (n = 3 independent differentiations, **p < 0.05, unpaired t test for significance comparing normalized quantities of TTR^{WT} and TTR^{L55P} error bars denote standard deviation).

(E) Upon addition of TMP, ATF6 target gene $HERPUD1$ was found to be significantly upregulated compared with DHFR.ATF6 HLCs in the absence of TMP. IRE1/XBP1s and PERK target genes $ERDJ4$ and $GADD34$, however, were not found to be differentially expressed in the presence of TMP. Positive control Tg was found to significantly upregulate expression of all UPR target genes tested (n = 6 independent differentiations, *p < 0.05, **p < 0.005, ****p < 0.0001, error bars denote standard deviation).

Several mechanisms could be responsible for the observed upregulation of *TF* in TTR^{L55P}-expressing HLCs. Firstly, expression could be linked to several pathways activated in response to the presence of destabilized TTR production. In line with this, regulation of *TF* has been linked to cytokine expression resulting from the negative acute-phase inflammatory response (Gruys et al., 2005), while at the same time expression of PERK target gene *GADD153* inversely correlates with *TF* expression (You et al., 2003). Mechanistically, it remains to be seen whether TTR aggregates intracellularly and in turn elicits stress response (as seen in α1-antitrypsin deficiency) (Chen et al., 2014). Alternatively, the gene signature identified in Figure 3 could include factors that directly or indirectly affect the transcription of *TF*. Under baseline conditions, transcription of *TF* is regulated by cell- and tissue-specific factors (e.g., HNF4a and CEBPα in liver and brain, respectively) (Espinosa de los Monteros et al., 1994; Zakin et al., 2002). It is therefore possible that the presence of TTR^{L55P} within HLCs affects the expression of *TF* via mechanisms distinct from those at work in other TTR-expressing tissues.

In addition to the differential expression of known and novel chaperone genes, we noted activation of the adaptive arms of the UPR (ATF6 and IRE1/XBP1s) in HLCs expressing mutant TTR. Together, these data indicate that the expression of TTR^{L55P} in iPSC-derived HLCs does not induce severe ER stress, but suggests that the activation of adaptive IRE1/XBP1s and ATF6 signaling observed in these cells reflects a protective mechanism to suppress secretion and subsequent aggregation of the destabilized TTR^{L55P} protein. Consistent with this, our immunoprecipitation-based LC-MS analysis of conditioned media from uncorrected HLCs showed that TTR^{L55P} levels were approximately 30% that of TTR^{WT} (Figure 2B). This result mirrors the lower levels of destabilized TTR mutants (as compared with wild-type TTR) observed in conditioned media prepared on HLCs expressing both variants (Chen et al., 2014, 2016; Genereux et al., 2015; Giadone et al., 2018; Leung et al., 2013; Leung and Murphy, 2016; Plate et al., 2016; Shoulders et al., 2013).

Our scRNA-seq data demonstrate activation of proteostasis transcriptional networks consisting of upregulation of chaperones as well as functional activation of adaptive UPR-associated signaling pathways in mutant HLCs. Wild-type ATTR amyloidosis, involving the misfolding and deposition of wild-type TTR in patients with no identified mutation, manifests around the eighth decade of life and is widely considered an aging-related disorder (Benson, 2012; Gertz et al., 2015; Ruberg and Berk, 2012). It is well-understood that proteostasis factors and the ability to cope with the production of misfolded proteins decreases with age while, similarly, iron has been shown to increase in a number of organs throughout aging (Bloomer et al.,

2008; Cook and Yu, 1998; Jung et al., 2008). Interestingly, since UPR signaling declines during normal aging (Hipp et al., 2019; Kaushik and Cuervo, 2015; Klaips et al., 2018; Labbadia and Morimoto, 2015), the presence of adaptive UPR signaling in the aforementioned HLCs derived from an individual with severe, early-onset disease could reflect protective biological pathways whose activity declines during the aging process. Aging-dependent reductions in adaptive UPR signaling could exacerbate TTR-associated ER stress and increase secretion of TTR in non-native conformations that facilitate toxic extracellular aggregation. Thus, monitoring changes in hepatic UPR activation and/or conformational stability of circulating TTR tetramers could reflect a potential biomarker to monitor progression of TTR amyloid disease pathogenesis (Schonhoft et al., 2017).

Together, these results indicate that the expression of a destabilized, aggregation-prone protein upregulates proteostasis factors and functionally activates adaptive UPR-associated signaling pathways in ATTR amyloidosis patient-specific iPSC-derived HLCs. Moreover, we demonstrated that inducible activation of ATF6 signaling in these cells resulted in a ~25% reduction of destabilized TTR^{L55P} while wild-type levels appeared unaffected. Though a relatively modest decrease, this reduction could represent a shift toward stability where properly folded, mutant TTRs form stabilized heterotetramers with wild-type TTRs (Rappley et al., 2014). Similar experiments, involving stress-independent activation of ATF6 signaling in 293T cells overexpressing destabilized TTR, implicated both ER-associated degradation and autophagy in degrading misfolded TTR, and in turn decreasing its secretion (Chen et al., 2014). Follow-up studies will be performed to understand the contribution of constituents of the gene signature in Figure 3 to employment of these pathways.

Conventional therapeutics for systemic amyloid diseases involve decreasing circulating levels of the amyloidogenic protein. In ATTR amyloidosis, for example, liver transplantation relies upon eliminating circulating levels of mutant TTR while RNAi-based therapeutics target and eliminate wild-type and mutant TTR transcripts (Adams et al., 2018; Benson et al., 2018; Butler et al., 2016; Buxbaum, 2018). Activating ATF6 signaling in ATTR amyloidosis HLCs could result in a therapeutic decrease in the secretion of misfolding-prone TTRs from the liver and thus a decrease in extracellular deposition of distal target tissue aggregates. Recent studies have demonstrated that selective activation of ATF6 signaling is achievable via addition of small molecules, while at the same time, upregulation of ATF6 signaling is relatively tolerated in humans with hyperactivating mutations (Chen et al., 2014; Glembotski et al., 2019; Romine and Wiseman, 2018; Shoulders et al., 2013). Future work will aim to further the development of

small-molecule-based ATF6-modulating compounds for the treatment of systemic amyloid diseases.

Together, these experiments challenge the long-held notion that ATTR amyloidosis livers are unaffected by the disease. Through the use of our iPSC-based model, we demonstrate that expression of amyloidogenic TTR results in transcriptional and functional changes in ATTR amyloidosis HLCs. Moreover, these data suggest that the liver employs protective mechanisms via adaptive UPR-associated signaling pathways to cope with the production of misfolding TTRs. Furthermore, this work demonstrates that modulation of UPR-associated ATF6 signaling results in a selective decrease in the secretion of misfolded proteins in patient-specific HLCs, potentially representing a broadly applicable therapeutic strategy for the complex and diverse systemic amyloid diseases.

EXPERIMENTAL PROCEDURES

TALEN-Mediated Gene Editing of Patient-Specific iPSCs

Cells were transfected via Lipofectamine with PLUS reagent (Thermo Fisher, cat. nos. 11668019, 11514015). In brief, iPSCs were cultured until ~60% confluent in a 6-well plate, and 1.2 μg of left and right TALEN targeting vectors and 3 μg of donor vector were added to cells. Puromycin (700 ng/μL) selection was then performed. Puromycin cassette excision was accomplished using transient transfection of the pHAGE-EF1α-Cre-IRES-Neo plasmid followed by subsequent screening and single-cell selection and expansion.

Directed Differentiation of iPSCs to Hepatocyte-like Cells

iPSCs were specified to the hepatic lineage via a 2D feeder-free, chemically defined differentiation protocol as previously described (Giadone et al., 2018; Gouon-Evans et al., 2006; Leung et al., 2013; Leung and Murphy, 2016; Szkolnicka and Hay, 2016).

MS Analysis of Secreted TTR

For immunoprecipitation-based MS (Figures 2B and S3B), TTR was pulled down from conditioned medium prepared on iPSC-derived hepatic lineages, as previously described (Giadone et al., 2018). Tandem mass tag (TMT) LC-MS/MS was utilized to directly detect the presence of the TTR^{L55P} peptide in conditioned hepatic supernatant. Additional details regarding these methodologies can be found in Supplemental Experimental Procedures.

Determining Downstream Neuronal Toxicity in Response to iPSC-Derived HLC Supernatant

Conditioned supernatant was generated by incubating hepatic differentiation media on day-16 HLCs for 72 h. Supernatant was collected and subsequently concentrated using Centrifugal Filter Units (Millipore Sigma, cat. no. UFC901024). (After first collection, cells were refed with medium for an additional 72 h to generate a second batch of conditioned supernatant.) Supernatant was first centrifuged at $200 \times g$ for 1 min at room temperature to remove cell debris. Medium was then collected, transferred to filter units, and spun at $2,140 \times g$ for 45 min at room temperature. Concentrated supernatant was subsequently stored at 4°C until dosing experiment. SH-SY5Y cells were plated at 2×10^5 cells and subsequently dosed for ~7 days with medium composed of SH-SY5Y growth medium and conditioned supernatant at a 1:1 ratio. Medium was replaced every 48 h until toxicity assay was performed. After dosing cells, floating and adherent SH-SY5Y cells were collected, stained with PI (BD Biosciences, cat. no. 556463), and analyzed via flow cytometry.

Analysis of Transcriptomic Data

Corrected and uncorrected cells were sorted and entered into the Fluidigm C1 HT workflow, which was used to capture and lyse individual cells, reverse transcribe RNA, and prepare libraries for sequencing (see Fluidigm protocol: Using the C1 High-Throughput IFC to Generate Single-Cell cDNA Libraries for mRNA Sequencing, cat. no. 100-9886; https://www.fluidigm.com/binaries/content/documents/fluidigm/resources/c1-mrna-seq-pr-100-7168/c1-mrna-seq-pr-100-7168/fluidigm%3Afile). Sequencing was performed on a Nextseq 500 using a high-output kit. Details regarding post hoc analysis of microarray data (Wilson et al., 2015) as well as our scRNA-seq experiment can be found in Supplemental Experimental Procedures.

XBP1 Splicing Assay

RNA was isolated from HLCs, and cDNA was generated via standard RT reaction. XBP1 transcript was amplified via PCR reaction with forward primer 5′-AAA CAG AGT AGC AGC TCA GAC TGC-3′ and reverse primer 5′-TCC TTC TGG GTA GAC CTC TGG GAG-3′. PCR program utilized included the following steps: 94°C for 4 min, 35 cycles of 94°C (10 s), 63°C (30 s), and 72°C (30 s), and lastly 72°C for 10 min. Amplified transcripts were subsequently digested with PstI enzyme (New England BioLabs, cat. no. R0140S) and analyzed on a 2.5% agarose gel. Relative quantities of bands were determined via ImageQuant TL software. For positive control for XBP1 activation, Tg (Millipore Sigma, cat. no. T9033) was added to undifferentiated iPSCs at a concentration of 1 μM for 24 h.

In Vitro Fibril Formation Assay

TTR^{L55P} fibril formation was triggered under mild acidic conditions. The amount of fibrils formed was measured by Congo red (CR) binding assay as reported previously (Klunk et al., 1989). TTR^{L55P} and lyophilized human plasma-derived apo-transferrin protein (Apo-TF; R&D Systems, cat. no. 3188-AT) resuspended in 10 mM sodium phosphate buffer (pH 7.8; 100 mM KCl, 1 mM EDTA) were both filtered through 0.2-μm membranes prior to their incorporation into the reaction mixtures. Addition of 50 mM sodium acetate buffer (pH 4.6) and 100 mM KCl lowered the pH of the reaction to 4.9. The final concentrations of TTR^{L55P} and Apo-TF were 0.2 mg/mL and 2,500 μg/mL, respectively. Fibril formation was carried out at 37°C without agitation in a mastercycler with lid temperature of 80°C to avoid condensation. Reactions were halted after 24 h with the addition of 1.5 M HEPES (pH 8.0). Finally, fibril formation reaction was added to 10 μM CR (Sigma-Aldrich, cat. no.

573-58-0) working dilution (prepared in 5 mM KH_2PO_4 [pH 7.4] and 150 mM NaCl). After 15 min at room temperature, absorbance was taken at 477 nm and 540 nm. The amount of CR bound to amyloid fibrils was determined via molar concentration of bound CR = $A_{540nm}/25,295 - A_{477nm}/46,306$. The percentage of fibrils formed was calculated via $\frac{TF + TTR^{L55P}_{t_{24}-t_0}}{TTR^{L55P}_{t_{24}-t_0}} \times$ 100. Information regarding production of recombinant human TTR^{L55P} can be found in Supplemental Experimental Procedures.

Generation of ATF6-Inducible TTR^{L55P} iPSC Line

TTR^{L55P} iPSCs were nucleofected (Lonza) with 3 μg of previously described DHFR.ATF6 donor construct (Chen et al., 2014) using the manufacturer's protocol. Forty-eight hours after nucleofection, cells were grown in 500 ng/μL puromycin for approximately 10 days. Successfully grown colonies were subjected to dilution cloning to ensure clonality. For assessment of functionality, clonal, puromycin-resistant colonies were subjected to 10 μM TMP for 48 h. RNA was harvested from each clone and qRT-PCR was performed to assess upregulation of the ATF6 target gene, *HSPA5*, in the presence of TMP.

DATA AND CODE AVAILABILITY

The dataset for the scRNA-seq experiment comparing corrected and uncorrected iPSC-derived HLCs (Figure 3) has been deposited under accession number GEO: GSE153541.

SUPPLEMENTAL INFORMATION

Supplemental Information can be found online at https://doi.org/10.1016/j.stemcr.2020.07.003.

REFERENCES

Ando, Y., Nakamura, M., and Araki, S. (2005). Transthyretin-related familial amyloidotic polyneuropathy. Arch. Neurol. *62*, 1057–1062.

Ando, Y., Sekijima, Y., Obayashi, K., Yamashita, T., Ueda, M., Misumi, Y., Morita, H., Machii, K., Ohta, M., Takata, A., et al. (2016). Effects of tafamidis treatment on transthyretin (TTR) stabilization, efficacy, and safety in Japanese patients with familial amyloid polyneuropathy (TTR-FAP) with Val30Met and non-Val30Met: a phase III, open-label study. J. Neurol. Sci. *362*, 266–271.

Adams, D., Gonzalez-Duarte, A., O'Riordan, W.D., Yang, C.C., Ueda, M., Kristen, A.V., Tournev, I., Schmidt, H.H., Coelho, T., Berk, J.L., et al. (2018). Patisiran, an RNAi therapeutic, for hereditary transthyretin amyloidosis. N. Engl. J. Med. *379*, 11–21.

Benson, M.D., Waddington-Cruz, M., Berk, J.L., Berk, J.L., Polydefkis, M., Dyck, P.J., Wang, A.K., Planté-Bordeneuve, V., Barroso, F.A., Merlini, G., et al. (2018). Inotersen treatment for patients with hereditary transthyretin amyloidosis. N. Engl. J. Med. *379*, 22–31.

Benson, M.D. (2012). Pathogenesis of transthyretin amyloidosis. Amyloid *19* (*Suppl 1*), 14–15.

Berk, J.L., Suhr, O.B., Obici, L., Sekijima, Y., Zeldenrust, S.R., Yamashita, T., Heneghan, M.A., Gorevic, P.D., Litchy, W.J., Wiesman, J.F., et al. (2013). Repurposing diflunisal for familial amyloid polyneuropathy: a randomized clinical trial. JAMA *310*, 2658–2667.

Blancas-Mejia, L.M., and Ramirez-Alvarado, M. (2013). Systemic amyloidoses. Ann. Rev. Biochem. *82*, 745–774.

Bloomer, S.A., Brown, K.E., Buettner, G.R., and Kregel, K.C. (2008). Dysregulation of hepatic iron with aging: implications for heat stress-induced oxidative liver injury. Am. J. Physiol. Regul. Integr. Comp. Physiol. *294*, R1165–R1174.

Butler, J.S., Chan, A., Costelha, S., Fishman, S., Willoughby, J.L., Borland, T.D., Milstein, S., Foster, D.J., Gonçalves, P., Chen, Q., et al. (2016). Preclinical evaluation of RNAi as a treatment for transthyretin-mediated amyloidosis. Amyloid *23*, 109–118.

Buxbaum, J.N., Tagoe, C., Gallo, G., Walker, J.R., Kurian, S., and Salomon, D.R. (2012). Why are some amyloidoses systemic? Does hepatic "chaperoning at a distance" prevent cardiac deposition in a transgenic model of human senile systemic (transthyretin) amyloidosis? FASEB J. *26*, 2283–2293.

Buxbaum, J.N. (2009). Animal models of human amyloidoses: are transgenic mice worth the time and trouble? FEBS Lett. *583*, 2663–2673.

Buxbaum, J.N. (2018). Oligonucleotide drugs for transthyretin amyloidosis. N. Engl. J. Med. *379*, 82–85.

Buxbaum, J.N. (2004). The systemic amyloidoses. Curr. Opin. Rheumatol. *16*, 67–75.

Buxbaum, J.N. (2019). Treatment of hereditary and acquired forms of transthyretin amyloidosis in the era of personalized medicine: the role of randomized controlled trials. Amyloid *26*, 55–65.

Chen, J.J., Genereux, J.C., Qu, S., Hulleman, J.D., Shoulders, M.D., and Wiseman, R.L. (2014). ATF6 activation reduces the secretion and extracellular aggregation of destabilized variants of an amyloidogenic protein. Chem. Biol. *21*, 1564–1574.

Chen, J.J., Genereux, J.C., Suh, E.H., Vartabedian, V.F., Rius, B., Qu, S., Dendle, M.T., Kelly, J.W., and Wiseman, R.L. (2016). Endoplasmic reticulum proteostasis influences the oligomeric state of an amyloidogenic protein secreted from mammalian cells. Cell Chem Biol 23, 1282–1293.

Cook, C.I., and Yu, B.P. (1998). Iron accumulation in aging: modulation by dietary restriction. Mech. Ageing Dev. 102, 1–13.

Ericzon, B.G., Holmgren, G., Lundgren, E., and Suhr, O.B. (2000). New structural information and update on liver transplantation in transthyretin-associated amyloidosis. Report from the 4th International Symposium on Familial Amyloidotic Polyneuropathy and Other Transthyretin Related Disorders & the 3rd International Workshop on Liver Transplantation in Familial Amyloid Polyneuropathy, Umea, Sweden, June 1999. Amyloid 7, 145–147.

Ericzon, B.G. (2007). Domino transplantation using livers from patients with familial amyloidotic polyneuropathy: should we halt? Liver Transpl. 13, 185–187.

Espinosa de los Monteros, A., Sawaya, B.E., Guillou, F., Zakin, M.M., de Vellis, J., and Schaeffer, E. (1994). Brain-specific expression of the human transferrin gene. similar elements govern transcription in oligodendrocytes and in a neuronal cell line. J. Biol. Chem. 269, 24504–24510.

Falk, R.H., Comenzo, R.L., and Skinner, M. (1997). The systemic amyloidoses. N. Engl. J. Med. 337, 898–909.

Gallagher, C.M., and Walter, P. (2016). Ceapins inhibit ATF6α signaling by selectively preventing transport of ATF6alpha to the Golgi apparatus during ER stress. eLife 5. https://doi.org/10.7554/eLife.11880.

Gallagher, C.M., Garri, C., Cain, E.L., Ang, K.K., Wilson, C.G., Chen, S., Hearn, B.R., Jaishankar, P., Aranda-Diaz, A., and Arkin, M.R. (2016). Ceapins are a new class of unfolded protein response inhibitors, selectively targeting the ATF6alpha branch. eLife 5. https://doi.org/10.7554/eLife.11878.

Genereux, J.C., Qu, S., Zhou, M., Ryno, L.M., Wang, S., Shoulders, M.D., Kaufman, R.J., Lasmézas, C.I., Kelly, J.W., and Wiseman, R.L. (2015). Unfolded protein response-induced ERdj3 secretion links ER stress to extracellular proteostasis. EMBO J. 34, 4–19.

Gertz, M.A., Benson, M.D., Dyck, P.J., Grogan, M., Coelho, T., Cruz, M., Berk, J.L., Plante-Bordeneuve, V., Schmidt, H.H., and Merlini, G. (2015). Diagnosis, prognosis, and therapy of transthyretin amyloidosis. J. Am. Coll. Cardiol. 66, 2451–2466.

Giadone, R.M., Rosarda, J.D., Akepati, P.R., Thomas, A.C., Boldbaatar, B., James, M.F., Wilson, A.A., Sanchorawala, V., Connors, L.H., Berk, J.L., and Wiseman, R.L. (2018). A library of ATTR amyloidosis patient-specific induced pluripotent stem cells for disease modelling and in vitro testing of novel therapeutics. Amyloid 25, 148–155.

Giunta, S., Galeazzi, R., Valli, M.B., Corder, E.H., and Galeazzi, L. (2004). Transferrin neutralization of amyloid beta 25-35 cytotoxicity. Clin. Chim. Acta 350, 129–136.

Glembotski, C.C., Rosarda, J.D., and Wiseman, R.L. (2019). Proteostasis and beyond: ATF6 in ischemic disease. Trends Mol. Med. 25, 538–550.

Gouon-Evans, V., Boussemart, L., Gadue, P., Nierhoff, D., Koehler, C.I., Kubo, A., Shafritz, D.A., and Keller, G. (2006). BMP-4 is required for hepatic specification of mouse embryonic stem cell-derived definitive endoderm. Nat. Biotechnol. 24, 1402–1411.

Gruys, E., Toussaint, M.J., Niewold, T.A., and Koopmans, S.J. (2005). Acute phase reaction and acute phase proteins. J. Zhejiang Univ. Sci. B 6, 1045–1056.

Hemming, A.W., Cattral, M.S., Chari, R.S., Greig, P.D., Lilly, L.B., Ashby, P., and Levy, G.A. (1998). Domino liver transplantation for familial amyloid polyneuropathy. Liver Transpl. 4, 236–238.

Herlenius, G., Wilczek, H.E., Larsson, M., and Ericzon, B.G. (2004). Ten years of international experience with liver transplantation for familial amyloidotic polyneuropathy: results from the Familial Amyloidotic Polyneuropathy World Transplant Registry. Transplantation 77, 64–71.

Hipp, M.S., Kasturi, P., and Hartl, F.U. (2019). The proteostasis network and its decline in ageing. Nat. Rev. Mol. Cell Biol. 20, 421–435.

Jacobson, D.R., McFarlin, D.E., Kane, I., and Buxbaum, J.N. (1992). Transthyretin Pro55, a variant associated with early-onset, aggressive, diffuse amyloidosis with cardiac and neurologic involvement. Hum. Genet. 89, 353–356.

Jung, S.H., DeRuisseau, L.R., Kavazis, A.N., and DeRuisseau, K.C. (2008). Plantaris muscle of aged rats demonstrates iron accumulation and altered expression of iron regulation proteins. Exp. Physiol. 93, 407–414.

Kan, H.W., Chiang, H., Lin, W.M., Yu, I.S., Lin, S.W., and Hsieh, S.T. (2018). Sensory nerve degeneration in a mouse model mimicking early manifestations of familial amyloid polyneuropathy due to transthyretin Ala97Ser. Neuropathol. Appl. Neurobiol. 44, 673–686.

Kaushik, S., and Cuervo, A.M. (2015). Proteostasis and aging. Nat. Med. 21, 1406–1415.

Klaips, C.L., Jayaraj, G.G., and Hartl, F.U. (2018). Pathways of cellular proteostasis in aging and disease. J. Cell Biol. 217, 51–63.

Klunk, W.E., Pettegrew, J.W., and Abraham, D.J. (1989). Quantitative evaluation of Congo red binding to amyloid-like proteins with a beta-pleated sheet conformation. J. Histochem. Cytochem. 37, 1273–1281.

Labbadia, J., and Morimoto, R.I. (2015). The biology of proteostasis in aging and disease. Annu. Rev. Biochem. 84, 435–464.

Lashuel, H.A., Wurth, C., Woo, L., and Kelly, J.W. (1999). The most pathogenic transthyretin variant, L55P, forms amyloid fibrils under acidic conditions and protofilaments under physiological conditions. Biochemistry 38, 13560–13573.

Leung, A., and Murphy, G.J. (2016). Multisystemic disease modeling of liver-derived protein folding disorders using induced pluripotent stem cells (iPSCs). Methods Mol. Biol. 1353, 261–270.

Leung, A., Nah, S.K., Reid, W., Ebata, A., Koch, C.M., Monti, S., Genereux, J.C., Wiseman, R.L., Wolozin, B., Connors, L.H., and Berk, J.L. (2013). Induced pluripotent stem cell modeling of multisystemic, hereditary transthyretin amyloidosis. Stem Cell Rep. 1, 451–463.

Li, X., Lyu, Y., Shen, J., Mu, Y., Qiang, L., Liu, L., Araki, K., Imbimbo, B.P., Yamamura, K.I., Jin, S., and Li, Z. (2018). Amyloid deposition in a mouse model humanized at the transthyretin and retinol-binding protein 4 loci. Lab. Invest. 98, 512–524.

Llado, L., Baliellas, C., Casasnovas, C., Ferrer, I., Fabregat, J., Ramos, E., Castellote, J., Torras, J., Xiol, X., and Rafecas, A. (2010). Risk of transmission of systemic transthyretin amyloidosis after domino liver transplantation. Liver Transpl. *16*, 1386–1392.

Loeffler, D.A., Connor, J.R., Juneau, P.L., Snyder, B.S., Kanaley, L., DeMaggio, A.J., Nguyen, H., Brickman, C.M., and LeWitt, P.A. (1995). Transferrin and iron in normal, Alzheimer's disease, and Parkinson's disease brain regions. J. Neurochem. *65*, 710–724.

Maurer, M.S., Elliott, P., Merlini, G., Shah, S.J., Cruz, M.W., Flynn, A., Gundapaneni, B., Hahn, C., Riley, S., Schwartz, J., and Sultan, M.B. (2017). Design and rationale of the phase 3 ATTR-ACT clinical trial (Tafamidis in Transthyretin Cardiomyopathy Clinical Trial). Circ. Heart Fail *10*, e003815.

Maurer, M.S., Schwartz, J.H., Gundapaneni, B., Elliott, P.M., Merlini, G., Waddington-Cruz, M., Kristen, A.V., Grogan, M., Witteles, R., and Damy, T. (2018). Tafamidis treatment for patients with transthyretin amyloid cardiomyopathy. N. Engl. J. Med. *379*, 1007–1016.

McCutchen, S.L., Colon, W., and Kelly, J.W. (1993). Transthyretin mutation Leu-55-Pro significantly alters tetramer stability and increases amyloidogenicity. Biochemistry *32*, 12119–12127.

Merlini, G., and Westermark, P. (2004). The systemic amyloidoses: clearer understanding of the molecular mechanisms offers hope for more effective therapies. J. Intern. Med. *255*, 159–178.

Misumi, Y., Narita, Y., Oshima, T., Ueda, M., Yamashita, T., Tasaki, M., Obayashi, K., Isono, K., Inomata, Y., and Ando, Y. (2016). Recipient aging accelerates acquired transthyretin amyloidosis after domino liver transplantation. Liver Transpl. *22*, 656–664.

Muchtar, E., Grogan, M., Dasari, S., Kurtin, P.J., and Gertz, M.A. (2017). Acquired transthyretin amyloidosis after domino liver transplant: phenotypic correlation, implication of liver retransplantation. J. Neurol. Sci. *379*, 192–197.

Niemietz, C., Fleischhauer, L., Sandfort, V., Guttmann, S., Zibert, A., and Schmidt, H.H. (2018). Hepatocyte-like cells reveal novel role of SERPINA1 in transthyretin amyloidosis. J. Cell Sci. *131*, jcs219824.

Ohta, M., Sugano, A., Hatano, N., Sato, H., Shimada, H., Niwa, H., Sakaeda, T., Tei, H., Sakaki, Y., Yamamura, K.I., and Takaoka, Y. (2018). Co-precipitation molecules hemopexin and transferrin may be key molecules for fibrillogenesis in TTR V30M amyloidogenesis. Transgenic Res. *27*, 15–23.

Plate, L., Cooley, C.B., Chen, J.J., Paxman, R.J., Gallagher, C.M., Madoux, F., Genereux, J.C., Dobbs, W., Garza, D., Spicer, T.P., and Scampavia, L. (2016). Small molecule proteostasis regulators that reprogram the ER to reduce extracellular protein aggregation. eLife *5*, e15550.

Raditsis, A.V., Milojevic, J., and Melacini, G. (2013). Aβ association inhibition by transferrin. Biophys. J. *105*, 473–480.

Rappley, I., Monteiro, C., Novais, M., Baranczak, A., Solis, G., Wiseman, R.L., Helmke, S., Maurer, M.S., Coelho, T., Powers, E.T., and Kelly, J.W. (2014). Quantification of transthyretin kinetic stability in human plasma using subunit exchange. Biochemistry *53*, 1993–2006.

Reixach, N., Deechongkit, S., Jiang, X., Kelly, J.W., and Buxbaum, J.N. (2004). Tissue damage in the amyloidoses: transthyretin monomers and nonnative oligomers are the major cytotoxic species in tissue culture. Proc. Natl. Acad. Sci. U S A *101*, 2817–2822.

Romine, I.C., and Wiseman, R.L. (2018). PERK signaling regulates extracellular proteostasis of an amyloidogenic protein during endoplasmic reticulum stress. Sci. Rep. *9*, 410.

Ruberg, F.L., and Berk, J.L. (2012). Transthyretin (TTR) cardiac amyloidosis. Circulation *126*, 1286–1300.

Schonhoft, J.D., Monteiro, C., Plate, L., Eisele, Y.S., Kelly, J.M., Boland, D., Parker, C.G., Cravatt, B.F., Teruya, S., Helmke, S., and Maurer, M. (2017). Peptide probes detect misfolded transthyretin oligomers in plasma of hereditary amyloidosis patients. Sci. Transl Med. *9*, 7621.

Shoulders, M.D., Ryno, L.M., Genereux, J.C., Moresco, J.J., Tu, P.G., Wu, C., Yates, I.I.I.J.R., Su, A.I., Kelly, J.W., and Wiseman, R.L. (2013). Stress-independent activation of XBP1s and/or ATF6 reveals three functionally diverse ER proteostasis environments. Cell Rep. *3*, 1279–1292.

Sousa, M.M., Fernandes, R., Palha, J.A., Taboada, A., Vieira, P., and Saraiva, M.J. (2002). Evidence for early cytotoxic aggregates in transgenic mice for human transthyretin Leu55Pro. Am. J. Pathol. *161*, 1935–1948.

Stangou, A.J., Heaton, N.D., and Hawkins, P.N. (2005). Transmission of systemic transthyretin amyloidosis by means of domino liver transplantation. N. Engl. J. Med. *352*, 2356.

Szkolnicka, D., and Hay, D.C. (2016). Concise review: advances in generating hepatocytes from pluripotent stem cells for translational medicine. Stem Cells *34*, 1421–1426.

Torres, S.E., Gallagher, C.M., Plate, L., Gupta, M., Liem, C.R., Guo, X., Tian, R., Stroud, R.M., Kampmann, M., Weissman, J.S., and Walter, P. (2019). Ceapins block the unfolded protein response sensor ATF6alpha by inducing a neomorphic inter-organelle tether. eLife *8*. https://doi.org/10.7554/eLife.46595.

Wechalekar, A.D., Gillmore, J.D., and Hawkins, P.N. (2016). Systemic amyloidosis. Lancet *387*, 2641–2654.

Wilson, A.A., Ying, L., Liesa, M., Segeritz, C.P., Mills, J.A., Shen, S.S., Jean, J., Lonza, G.C., Liberti, D.C., Lang, A.H., and Nazaire, J. (2015). Emergence of a stage-dependent human liver disease signature with directed differentiation of alpha-1 antitrypsin-deficient iPS cells. Stem Cell Rep. *4*, 873–875.

Yamamoto, S., Wilczek, H.E., Iwata, T., Larsson, M., Gjertsen, H., Söderdahl, G., Solders, G., and Ericzon, B.G. (2007). Long-term consequences of domino liver transplantation using familial amyloidotic polyneuropathy grafts. Transpl. Int. *20*, 926–933.

Yang, N., Zhang, H., Wang, M., Hao, Q., and Sun, H. (2012). Iron and bismuth bound human serum transferrin reveals a partially-opened conformation in the N-lobe. Sci. Rep. *2*, 999.

You, K.R., Liu, M.J., Han, X.J., Lee, Z.W., and Kim, D.G. (2003). Transcriptional regulation of the human transferrin gene by GADD153 in hepatoma cells. Hepatology *38*, 745–755.

Zakin, M.M., Baron, B., and Guillou, F. (2002). Regulation of the tissue-specific expression of transferrin gene. Dev. Neurosci. *24*, 222–226.